Removal of Carbon Dioxide from Natural Gas by Vacuum Pressure Swing Adsorption

Simone Cavenati, Carlos A. Grande, and Alírio E. Rodrigues*

Laboratory of Separation and Reaction Engineering (LSRE), Department of Chemical Engineering, Faculty of Engineering, University of Porto, Rua Dr. Roberto Frias, s/n, 4200-465, Porto, Portugal

Received March 23, 2006. Revised Manuscript Received August 16, 2006

A vacuum pressure swing adsorption (VSA-PSA) process is studied for the removal of carbon dioxide in a contaminated stream of natural gas to achieve fuel grade methane. The adsorbent used was zeolite 13X (CECA) where CO_2 is strongly adsorbed. A Skarstrom-type cycle comprising pressurization with product, feed, countercurrent blowdown, and countercurrent purge was employed. A mixture having 60% CH_4/20% CO_2/20% N_2 was used, and two different temperatures were evaluated in a single-column VSA-PSA unit. Under the conditions tested, CO_2 was removed to levels lower than 2% as required by fuel grade methane with methane recovery higher than 80% without recycle. This separation process also helps in the CH_4-N_2 separation. A bidisperse (macropore−micropore) model also including distributed energy balances in gas, solid, and column wall considering heat and mass transfer resistance at the gas−solid interface was used to simulate the VSA-PSA behavior and compare with experiments. Also, some scale-up considerations are considered and evaluated by simulations of the process.

1. Introduction

Natural gas (NG) is composed by high concentrations of methane (>80%), with other hydrocarbons (C_{2+}) in variable quantities and several impurities in smaller quantities, often nitrogen and carbon dioxide. The proportion of contaminants is specific for each geological formation and may have important variations even in a single region. In many cases, the contamination with CO_2 exceeds the tolerable values, as some sources in Germany (Pannonian Basin) or in Australia (Cooper−Eromanga basin).[1] Also, naturally occurring nitrogen (NON) can be a serious contaminant in NG streams. The reduction of carbon dioxide is critical for transportation and usage to prevent corrosion of equipment and pipelines. Many countries established standard rules for the concentration of contaminants for transportation of NG through pipelines. When the natural gas meets such specifications, it is called "pipeline quality methane" and can be inserted in pipelines, increasing its market and commercial value. Although the concentration of contaminants is variable according to different regulations, typically the content of inert gas (nitrogen) has maximum values between 2 and 4% while the content of CO_2 cannot exceed 2%.

Actually, natural gas fields are equipped with some technology for the removal of carbon dioxide, either for the separation of the CO_2 existing in the original composition of the gas or for the removal of the CO_2 injected for enhanced oil recovery (EOR) to increase the field performance. There are three technologies that dominate the market:

(1) *Chemical absorption*: This process use monoethanolamine (MEA) or another alkanolamine or even a combination of amines to remove CO_2 from the stream. NG is sweetened in a tower at temperatures around 323 K, and then, the alkanolamine is regenerated at temperatures around 383−393 K.[2] Although the process is well-known, it has many problems of corrosion of the MEA with contaminants[3] and the cost of operation is high due to the large amounts of energy employed in solvent regeneration.

(2) *Physical absorption*: This process employs other kind of solvents (glycols or other organic solvents) where the interaction with CO_2 or any other acid gas is not as strong as with alkanolamines and where less energy is employed in regeneration.

(3) *Cryogenic distillation*: Reducing the temperature of the natural gas stream, carbon dioxide will liquefy at temperatures much higher than methane being removed in an intermediate step. This is an attractive technology when NG is going to be transported in the form of LNG (liquefied natural gas). This process has the additional advantage of separating the water and carbon dioxide.[4] Approximately 25% of the natural gas produced in the world is transported as LNG,[5] since the volume is reduced around 600 times.

These three alternatives consume large amounts of energy and are more appropriate to fields where large volumes of NG are processed due to economical constraints. For the case of medium and small volumes of gas to be processed, other alternatives such as adsorption-based processes may improve the overall economics due to lower operating costs. Adsorption-based technologies can reduce the energy needed for the regeneration of the separation agent (adsorbent) and may have a higher degree of automation.

In the last years, the removal of contaminants from natural gas streams by PSA was intensively studied, mainly because

* To whom correspondence should be addressed. Phone: +351 22 508 1671. Fax: +351 22 508 1674. E-mail: arodrig@fe.up.pt.

(1) Krooss, B. M.; Van Bergen, F.; Gensterblum, Y.; Siemons, N.; Pagnier, H. J. M.; David, P. Coals. *Int. J. Coal Geol.* **2002**, *51*, 69−92.

(2) US EPA. *Coalbed Methane Outreach Program Technical and Economic Assessment of Potencial to Upgrade Gob Gas to Pipeline Quality*; Report 430-R-97-012, 1997.

(3) Rao, A. B.; Rubin, E. S. *Environ. Sci. Technol*. **2002**, *36*, 4467−4475.

(4) Markovs, J.; James, E. F., Jr. Process for Purifying Natural Gas. US Patent 5,089,034, 1992.

(5) Gerasimov, V. E.; Pederel'skii, V. A.; Lyapin, A. I.; Darbinyan, R. V.; Dovbish, A. L. *Chem. Pet. Eng*. **2004**, *40*, 339−343.

10.1021/ef060119e CCC: $33.50
Published on Web 09/20/2006

of the contributions of the Engelhard Corporation with the Molecular Gate technology using their patented adsorbents (Engelhard titanosilicates) for the removal of water, carbon dioxide, and nitrogen [6−8].

Adsorption processes for the removal of CO_2 from NG streams are based on materials with selective adsorption to CO_2 by different equilibrium capacities or by differences in uptake rates. Pressure swing adsorption (PSA) is one of the most known industrial processes for gas separation.[9] PSA technology was already suggested for the removal of CO_2 from gaseous streams containing methane.[10] The most important decision in any adsorption-based technology is the adsorbent selection. Zeolites are microporous materials that adsorb CO_2 strongly, suggesting that these materials can be used in PSA processes.[11] Zeolites have proved to have better performance than activated carbons in the PSA separation of CO_2 from flue gases.[12]

This paper deals with CO_2 removal from a highly contaminated stream of natural gas containing 60% CH_4, 20% CO_2, and 20% N_2 (simulating a high NON contamination). The objective is to reduce carbon dioxide content to achieve pipeline specifications for transport (content of CO_2 < 2%). The product of this separation process should go to another process to remove nitrogen (nitrogen rejection unit, NRU) before being injected into the pipeline network. The process studied was vacuum pressure swing adsorption (VSA-PSA) using zeolite 13X as the selective adsorbent for CO_2. A Skarstrom-type cycle comprising pressurization, feed, countercurrent blowdown, and countercurrent purge with product was employed. Experiments in a single-column PSA unit were performed at ambient temperature (299 K) and 323 K with different step times and simulated using a bidisperse model with distributed energy balances. Simulations for a VSA-PSA unit operating in the adiabatic regime were also performed, and some scale-up aspects of this process will be discussed.

2. Experimental Section

The VSA-PSA experimental setup is composed of a single column unit that operates under un-steady-state conditions simulating the real operation of a single column in a continuous multicolumn VSA-PSA. The equipment is connected to a computer where individual gas flowrates exiting the column and pressures at the inlet and outlet of the column are stored. The temperature inside the column is measured at three different points: 0.17, 0.43, and 0.68 m from the feed inlet. The complete equipment setup was reported elsewhere.[13]

The molar flowrate of gases exiting the column was analyzed via a multiport valve system where 11 samples can be stored for subsequent analysis in a gas chromatograph (Chrompack 9000, Netherlands) with thermal conductivity and flame ionization detectors in series. The column used in the gas chromatography (GC) was a CP-Poraplot Q (Varian, Netherlands) with a flowrate of 7.0 mL/min of helium (used as the carrier gas and thermal conductivity detection (TCD) reference gas) at a constant temperature of 313 K. The error in the concentration measurements is ±2%. The scheme of the experimental setup is depicted in Figure 1.

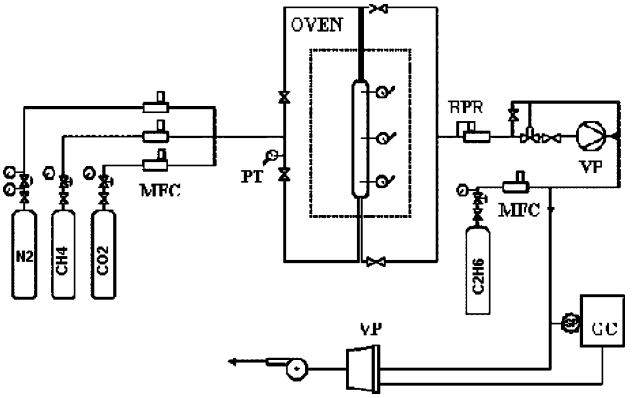

Figure 1. Scheme of the laboratory pressure swing adsorption (PSA) unit used in this work: PT, pressure transducer; BPR, back pressure regulator; MFC, mass flow controllers; GC, gas chromatograph; VP, vacuum pump.

Table 1. Adsorbent Physical Properties and Details of the Column Used in the VSA-PSA Benchmark Experiments for Removal of CO_2 from $CH_4/CO_2/N_2$ Mixtures Using Zeolite 13X (CECA)

column radius, m	0.0105
column length, m	0.83
column porosity	0.33
column density, kg/m^3	756.46
density of column wall, kg/m^3	8238
specific heat of the column wall, J/kg·K	500
extrudate radius (infinite cylinder), m	0.8×10^{-3}
extrudate density, kg/m^3	1130
extrudate porosity	0.54
extrudate tortuosity (estimated)	2.2
adsorbent specific heat, J/kg·K	920

The adsorbent employed in this study was zeolite 13X, kindly provided by CECA (Paris, France). The adsorbent extrudates were stored in the VSA-PSA column and activated overnight at 593 K under a small flow of helium. The heating rate to reach this temperature was 1 K/min. This activation protocol proved to be effective to desorb water for reliable adsorption equilibrium determinations.[14] The adsorption equilibrium of pure gases on zeolite 13X used in this work was already reported.[14] The physical properties of the adsorbent together with the details of the fixed-bed column (of the VSA-PSA experiments) used in all the experiments are shown in Table 1.

All gases used in this report were provided by Air Liquide and used as received: methane N35, carbon dioxide N24, nitrogen N50, and helium N50 (purity greater than 99.95, 99.4, and 99.999%, respectively).

3. Modeling and Simulations

To describe the fixed bed behavior of the ternary mixture of $CH_4/CO_2/N_2$, we have used a mathematical model with the following assumptions:

(a) Ideal gas behavior exists in all the steps of the process.

(b) Heat, mass, and momentum transport in the radial direction of the column are neglected and only the axial coordinate is considered.

(c) The momentum balance is simplified by using the Ergun equation.

(d) Three energy balances were employed to describe heat transfer in the gas phase, solid phase, and column wall.

(e) Macropore and micropore diffusion equations are simplified by a bi-LDF (linear driving force) model instead of the

(6) Kuznicki, S. M.; Bell, V. A.; Desai, B. T.; Petrovic, I. Separation of Nitrogen from Mixtures thereof with Methane Utilizing Barium Exchanged ETS-4. U.S. Patent 5,989,316, 1999.

(7) Kuznicki, S. M.; Bell, V. A.; Desai, B. T.; Petrovic, I. Small-pored Crystallyine Titanium Molecular Sieve Zeolites and their use in Gas Separation Processes. U.S. Patent 6,068,682, 2000.

(8) Dolan W. B.; Mitariten, M. J. Heavy Hydrocarbon Recovery from Pressure Swing Adsorption Unit Tail Gas. U.S. Patent 6,610,124, 2003.

(9) Sircar, S. *Ind. Eng. Chem. Res.* **2002**, *41*, 1389−1392.

(10) Sircar, S. Adsorption and Ion Exchange. *AIChE Symp. Ser.* **1988**, *84*, 70−72.

(11) Siriwardane, R. V.; Shen, M.-S.; Fisher, E. P. *Energy Fuels* **2001**, *15*, 279−284.

(12) Chue, K. T.; Kim, J. N.; Yoo, Y. J.; Cho, S. H.; Yang, R. T. *Ind. Eng. Chem. Res.* **1995**, 34, 591−598.

(13) Da Silva, F. A. Cyclic Adsorption Processes: Application to Propane/Propylene Separation. Ph.D. Thesis, University of Porto, Portugal, 1999.

(14) Cavenati, S.; Grande, C. A.; Rodrigues, A. E. *J. Chem. Eng. Data* **2004**, *49*, 1095−1101.

Table 2. Adsorption Equilibrium and Diffusion Parameters of Pure CH_4, CO_2, and N_2 in Zeolite 13X Extrudates[a]

gas	$q_{max,i}$ (mol/kg)	K_i^0 (1/kPa)	a_i (−)	$-\Delta H_i$ (kJ/mol)	$D_{p,i}/R_p^2$ (1/s)[b]	$D_{\mu,i}$ (m^2/s)[c]
CH_4	28.871	4.34×10^{-1}	8.136	15.675	1.47×10^{-2} (301 K)	3.00×10^{-8} (301 K)
					1.64×10^{-2} (323 K)	3.30×10^{-8} (323 K)
CO_2	17.901	3.20×10^{-5}	13.120	54.729	1.23×10^{-2} (301 K)	3.92×10^{-15} (301 K)
					1.35×10^{-2} (323 K)	5.35×10^{-15} (323 K)
N_2	29.676	1.79×10^{-1}	7.917	15.716	1.76×10^{-2} (301 K)	3.00×10^{-9} (301 K)
					1.96×10^{-2} (323 K)	4.00×10^{-9} (323 K)

[a] Adsorption equilibrium parameters were previously reported.[17] [b] Estimated using the Bosanquet equation shown in the mathematical model. [c] Values obtained from the literature.[15,16]

Table 3. Mathematical Model Used in VSA-PSA Modeling for Separation of $CH_4/CO_2/N_2$ with Zeolite 13X

component mass balance	$\epsilon_c \frac{\partial C_i}{\partial t} = \epsilon_c \frac{\partial}{\partial z}\left(D_{ax} C_t \frac{\partial y_i}{\partial t}\right) - \frac{\partial (u_i C_i)}{\partial z} - (1-\epsilon_c)\frac{a' k_{fi}}{Bi_i + 1}(C_i - \bar{c}_i)$
Ergun eq	$\frac{\partial P}{\partial z} = -\frac{150\mu_g(1-\epsilon_c)^2}{\epsilon_c^3 d_p^2} u_i + \frac{1.75(1-\epsilon_c)\rho_g}{\epsilon_c^3 d_p}\lvert u_i\rvert u_i$
LDF eq for the macropores	$\epsilon_p \frac{\partial \bar{c}_i}{\partial t} + \rho_p \frac{\partial \langle \bar{q}_i \rangle}{\partial t} = \epsilon_p K_{p,i} \frac{Bi_i}{Bi_i + 1}(C_i - \bar{c}_i) \quad K_{p,i} = \frac{8 D_{p,i}}{R_p^2}$
LDF eq for the micropores	$\frac{\partial \langle \bar{q}_i \rangle}{\partial t} = K_{\mu,i}(q_i^* - \langle \bar{q}_i \rangle) \quad K_{\mu,i} = \frac{15 D_{\mu,i}}{r_c^2} \quad D_{\mu,i} = D_{\mu,i}^0 \exp(-E_{a,i}/R_g T_g)$
gas-phase energy balance	$\epsilon_c C_t \tilde{C}_v \frac{\partial T_g}{\partial t} = \frac{\partial}{\partial z}\left(\lambda \frac{\partial T_g}{\partial z}\right) - u_i C_t \tilde{C}_p \frac{\partial T_g}{\partial z} + \epsilon_c R_g T_g \frac{\partial C_t}{\partial t} - (1-\epsilon_c) a' h_f (T_g - T_s) - \frac{2 h_w}{R_w}(T_g - T_w)$
solid-phase energy balance	$(1-\epsilon_c)[\epsilon_p \sum_{i=1}^{n} \bar{c}_i \tilde{C}_{vi} + \rho_p w_c \sum_{i=1}^{n} \langle \bar{q}_i \rangle \tilde{C}_{v,ads,i} + \rho_p \tilde{C}_{ps}] \frac{\partial T_s}{\partial t} = (1-\epsilon_c)\epsilon_p R_g T_s \frac{\partial \bar{c}_i}{\partial T} + \rho_b \sum_{i=1}^{n} (-\Delta H_i) \frac{\partial \langle \bar{q}_i \rangle}{\partial t} + (1-\epsilon_c) a' h_f (T_g - T_s)$
wall energy balance	$\rho_w \tilde{C}_{pw} \frac{\partial T_w}{\partial t} = \alpha_w h_w (T_g - T_w) - \alpha_{wl} U (T_w - T_\infty)$ $\alpha_w = \frac{D_w}{e(D_w + e)} \quad \alpha_{wl} = \frac{1}{(D_w + e)\ln\left(\frac{D_w + e}{D_w}\right)}$
multisite Langmuir isotherm	$\left(\frac{q_i^*}{q_{max,i}}\right) = K_i P y_i \left[1 - \sum_i \left(\frac{q_i^*}{q_{max,i}}\right)\right]^{a_i} \quad K_i = K_i^0 \exp(-\Delta H_i / R_g T_s)$
Bosanquet eq	$\frac{1}{D_{p,i}} = \tau_p \left(\frac{1}{D_{m,i}} + \frac{1}{D_{k,i}}\right)$

mass balances in the macropores and in the zeolite crystals. This assumption has a large impact in computational time.

(f) A film mass transfer in the layer surrounding the pellets is considered.

(g) The void fraction is uniform in the entire column.

(h) Crystal diffusivity coefficients at infinite dilution used in the model were obtained from literature.[15,16] The micropore diffusivity coefficients have an exponential dependence with temperature. Values are detailed in Table 2. Diffusion of these gases in zeolite 13X was very fast and in commercial pellets or extrudates is normally controlled by diffusion in the macropores of the inert matrix containing the zeolite crystals estimated using the Bosanquet equation.

(i) The multisite-Langmuir model describes the adsorption equilibrium behavior of the mixture with parameters (see Table 2) taken from pure component data.[17] The maximum amount adsorbed of each gas was imposed by the thermodynamic constraint $a_i q_{max,i}$ = constant. The parameters reported in Table 2 are merely fitting parameters, and no physical meaning was attributed to them. The high equilibrium selectivity of zeolite 13X toward CO_2 can be observed in the adsorption equilibrium isotherms of pure gases at 299 and 308 K, as shown in Figure 2.

The complete model equations used for description of the VSA-PSA process are detailed in Table 3. Boundary and initial conditions employed both in VSA-PSA experiments and simulations are described in Table 4.

The performance of the different experiments and simulations was evaluated according to three basic parameters: purity and

(15) Caro, J.; Bulow, M.; Karger, J. *Chem. Eng. Sci.* **1985**, *40*, 2169−2170.

(16) Bar, N. K.; McDaniel, P. L.; Coe, C. G.; Seiffert, G.; Karger, J. *Zeolites* **1997**, *18*, 71−74.

(17) Cavenati, S. Separação de Misturas $CH_4/CO_2/N_2$ por Processos Adsorptivos. Ph.D. Thesis, University of Porto, Portugal, 2005.

Table 4. Boundary and Initial Conditions of VSA-PSA Process for $CH_4/CO_2/N_2$ Separation Using Zeolite 13X

Countercurrent Pressurization with Methane

$$u(0) = 0 \qquad P(L_c) = P_{inlet}$$

$$\frac{\partial y(i,0)}{\partial z}|_{z^-} = 0 \qquad \frac{\epsilon D_{ax}}{u(L_c)}\frac{\partial y(i,L_c)}{\partial z}|_{z^-} - y(i,L_c)|_{z^-} + y(i,L_c)|_{z^+} = 0$$

$$\frac{\partial T_g(0)}{\partial z}|_{z^-} = 0 \qquad \lambda\frac{\partial T_g(L_c)}{\partial z}|_{z^-} - uC\tilde{C}_p T_g(L_c)|_{z^-} + uC\tilde{C}_p T_g(L_c)|_{z^+} = 0$$

Feed Step

$$u(0)C(i,0)|_{z^+} = u(0)C(i,0)|_{z^-} \qquad P(L_c) = P_{exit}$$

$$\frac{\epsilon D_{ax}}{u(0)}\frac{\partial y(i,0)}{\partial z}|_{z^+} - y(i,0)|_{z^+} + y(i,0)|_{z^-} = 0 \qquad \frac{\partial y(i,L_c)}{\partial z}|_{z^-} = 0$$

$$\lambda\frac{\partial T_g(0)}{\partial z}|_{z^+} - uC\tilde{C}_p T_g(0)|_{z^+} + uC\tilde{C}_p T_g(0)|_{z^-} = 0 \qquad \frac{\partial T_g(L_c)}{\partial z}|_{z^-} = 0$$

Countercurrent Blowdown

$$P(0) = (P_{feed} - P_{blow})\exp(-0.1t - (N-1)t_{total} - (t_{press} + t_{feed})) + P_{blow} \qquad u(L_c) = 0$$

$$\frac{\partial y(i,0)}{\partial z}|_{z^-} = 0 \qquad \frac{\partial y(i,L_c)}{\partial z}|_{z^-} = 0$$

$$\frac{\partial T_g(0)}{\partial z}|_{z^+} = 0 \qquad \frac{\partial T_g(L_c)}{\partial z}|_{z^-} = 0$$

Countercurrent Purge with Methane

$$P(0) = P_{exit} \qquad u(L_c)C(i,L_c)|_{z^+} = u(L_c)C(i,L_c)|_{z^-}$$

$$\frac{\partial y(i,0)}{\partial z}|_{z^-} = 0 \qquad \frac{\epsilon D_{ax}}{u(L_c)}\frac{\partial y(i,L_c)}{\partial z}|_{z^-} - y(i,L_c)|_{z^-} + y(i,L_c)|_{z^+} = 0$$

$$\frac{\partial T_g(0)}{\partial z}|_{z^-} = 0 \qquad \lambda\frac{\partial T_g(L_c)}{\partial z}|_{z^-} - uC\tilde{C}_p T_g(L_c)|_{z^-} + uC\tilde{C}_p T_g(L_c)|_{z^+} = 0$$

Initial Conditions of the VSA-PSA Column

$$q(i,z) = 0$$

$$T_g(z) = T_s(z) = T_w(z) = 301\ \text{K}$$

$$P(z) = 120\ \text{kPa}$$

$$y(CH_4,z) = y(CO_2,z) = y(N_2,z) = 0; \quad y(He,z) = 1$$

recovery of product and unit productivity of the PSA. They are defined by

$$\text{PURITY} = \frac{\int_0^{t_{feed}} C_{CH4}u|_{z=L}\,dt}{\left(\int_0^{t_{feed}} C_{CH4}u|_{z=L}\,dt + \int_0^{t_{feed}} C_{CO2}u|_{z=L}dt + \int_0^{t_{feed}} C_{N2}u|_{z=L}\,dt\right)} \quad (1)$$

$$\text{RECOVERY} = \frac{\int_0^{t_{feed}} C_{CH4}u|_{z=L}\,dt - \int_0^{t_{press}} C_{CH4}u|_{z=L}\,dt - \int_0^{t_{purge}} C_{CH4}u|_{z=L}\,dt}{\int_0^{t_{feed}} C_{CH4}u|_{z=0}\,dt} \quad (2)$$

$$\text{PRODUCTIVITY} = \frac{\left(\int_0^{t_{feed}} C_{CH4}u|_{z=L}\,dt - \int_0^{t_{press}} C_{CH4}u|_{z=L}dt - \int_0^{t_{purge}} C_{CH4}u|_{z=L}\,dt\right)A_{col}}{t_{cycle}w_{ads}} \quad (3)$$

where w_{ads} is the adsorbent mass loaded in the column, A_{col} is the area of the column, and t_{press}, t_{feed}, and t_{purge} are the times of the pressurization, feed, and countercurrent blowdown and purge steps, respectively, while t_{cycle} ($= t_{press} + t_{feed} + t_{blow} + t_{purge}$) is the total cycle time.

For the simulations of the VSA-PSA process, mass, energy, and momentum balances were solved simultaneously using the gPROMS (PSE, UK) package. This model was solved using the orthogonal collocation method on finite elements (OCFE) with 50 finite elements and two interior collocation points in each element of the adsorption bed.

4. Results and Discussion

4.1. Verification of Fixed-Bed Mathematical Model: Ternary Breakthrough Curves. The mathematical model described in Table 3 has several mass and energy transport parameters that were calculated from correlations from the literature.[18−20] The applicability of these calculated transport parameters must be checked. Before starting with the experi-

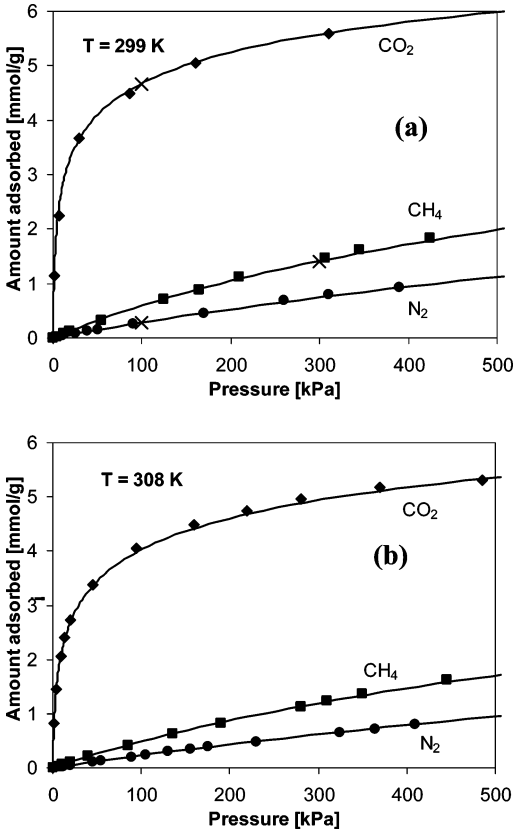

Figure 2. Adsorption equilibrium of CO_2, CH_4, and N_2 on zeolite 13X (CECA)[14] at 299 (a) and 308 K (b). The crosses in a indicates the amount adsorbed for a mixture of 20% CO_2/60% CH_4/20% N_2 at a feed pressure of 500 kPa.

mental PSA results, fixed bed runs were used as "mathematical model verification" experiments, where calculated values of the mass and energy parameters are inserted in the program for future use in PSA simulations. These experiments were also used to determine the only fitting parameter of the model which was the heat transfer coefficient at the wall (h_w).

The first experiment was a breakthrough experiment using only carbon dioxide with a total pressure in the column of 320 kPa at 299 K using a flowrate of 2.07 SLPM (liters per minute under the standard conditions of 298 K and 1 atm). An initial flowrate of helium was switched to a CO_2 stream at time $t = 0$. This experiment allows us to check the CO_2 capacity and its diffusivity in the zeolite extrudates. The results of this experiment (molar flow of CO_2 exiting the column and temperature profiles at 0.17, 0.43, and 0.68 m from feed inlet) are shown in Figure 3 where symbols correspond to experimental points and lines to the simulations using the mathematical model proposed. It can be observed that the column has a very large capacity to adsorb CO_2. Another interesting point is the temperature increase higher than 70 K due to the release of the heat of adsorption of CO_2 in zeolite 13X. Note that the temperature measured in the top of the column corresponds to the measurement in the column wall and not inside the column. To improve the predictions of the large temperature excursions in the column, three energy

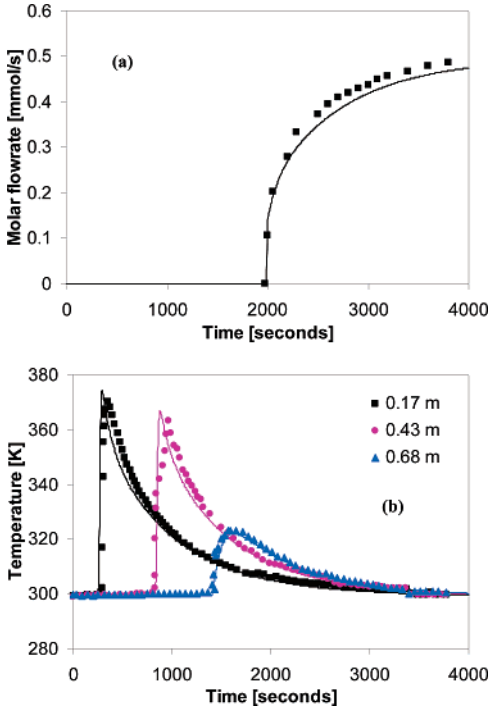

Figure 3. Breakthrough curve of CO_2 in zeolite 13X (CECA). The experimental conditions are as follows: temperature = 299 K; feed flowrate = 2.07 SLPM; pressure = 320 kPa. (a) Molar flowrate of CO_2 exiting the column. (b) Temperature profiles at three different positions inside the column (0.17, 0.43, and 0.68 m from the feed inlet). The symbols correspond to experimental data, and the lines are predictions of the mathematical model proposed.

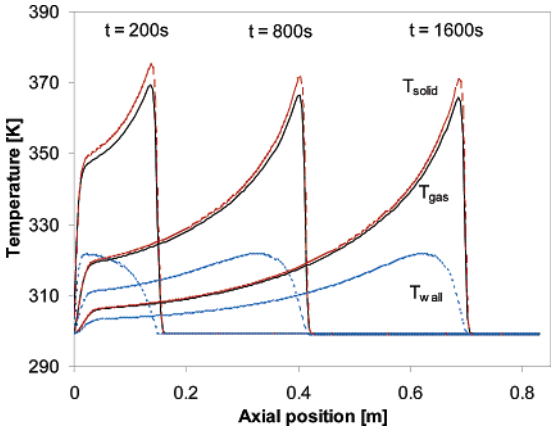

Figure 4. Simulated temperature profiles of the solid phase, gas phase, and column wall at three different times (t = 200, 800, and 1600 s) for the CO_2 breakthrough curve in zeolite 13X.

balances were used in the mathematical model. The difference between the temperature of the solid phase (adsorbent), gas phase, and column are shown in Figure 4 for different times (t = 200, 800, and 1600 s) inside the column. As can be observed, the temperature of the solid is very close to the temperature of the gas phase (±3 K). In a PSA process, according to the shape of the isotherms of CO_2, the increase of temperature in the cyclic steady state is much smaller than in the first cycle, and for this reason, further simplification of the mathematical modeling can be applied to this system.

Two different ternary breakthrough experiments were performed at different temperatures: ambient temperature (299 K) and 323 K. In both experiments, a flow of helium was changed (at time $t = 0$) to a feed stream containing 60% CH_4/20% CO_2/20% N_2. The results of the breakthrough curves at 299 and 323

(18) Ruthven, *D. M. Principles of Adsorption & Adsorption Processes*; John Wiley & Sons: New York, 1984.
(19) Incropera, F. P.; De Witt, D. P. *Fundamentals of Heat and Mass Transfer*; John Wiley: New York, 1996.
(20) Bird, R. B.; Stewart, W. E.; Lightfoot, E. N. *Transport Phenomena*, 2nd ed.; Wiley International: Singapore, 2002.
(21) Cavenati, S.; Grande, C. A.; Rodrigues, A. E. *Chem. Eng. Sci.* **2006**, *61*, 3893−3906.

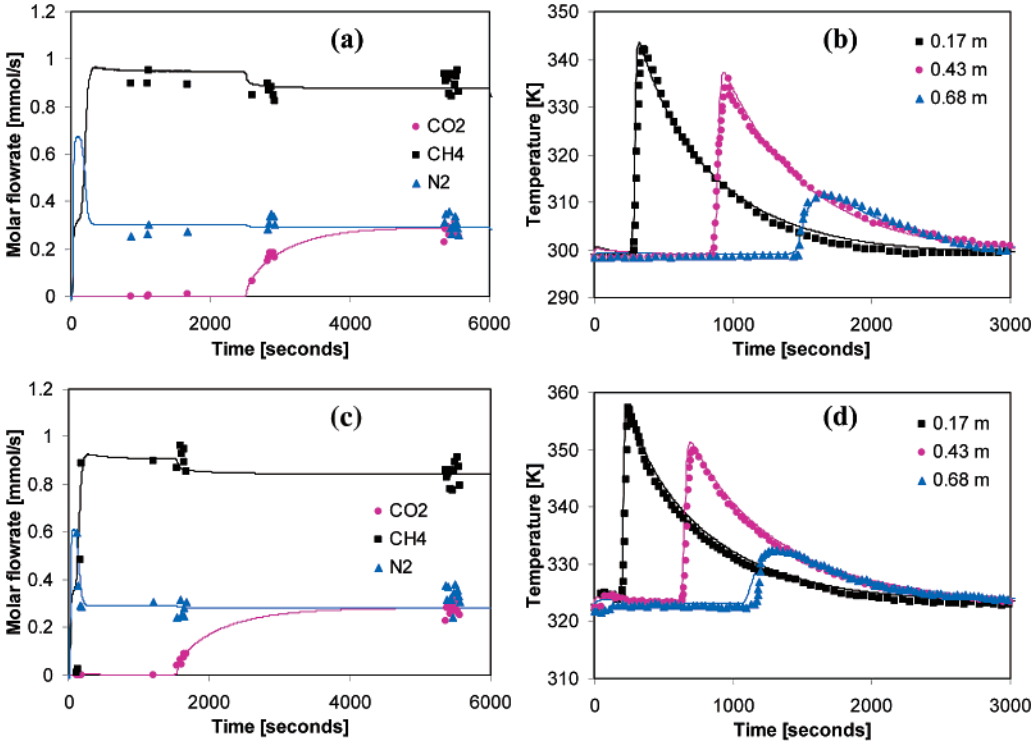

Figure 5. Breakthrough curves of 60% CH_4/20% CO_2/20% N_2 in zeolite 13X (CECA). (a and b) Molar flowrate at the exit of the column and temperature profiles for the run at 299 K. (c and d) Molar flowrate at the exit of the column and temperature profiles for the run at 323 K.

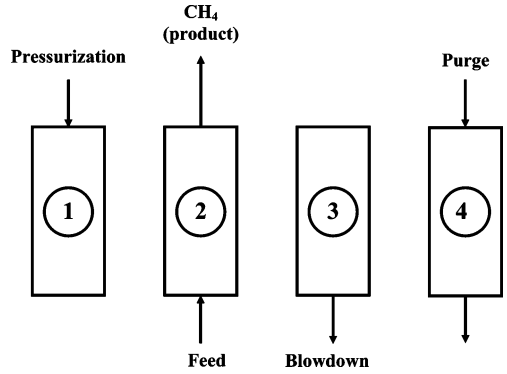

Figure 6. Schematic diagram of the four-step PSA cycle used in the benchmark experiments.

K are reported in Figure 5. The predictions of the mathematical model proposed with the diffusivities obtained from the literature and the heat transfer coefficient at the wall determined in the experiment using only CO_2 were in agreement with the experimental results. In both experiments, the concentration front of CO_2 at the exit of the column was dispersed by the temperature changes inside the column. In the experiment at 299 K, the ratios of the amounts adsorbed were $q_{CH4}/q_{CO2} = 0.075$ and $q_{N2}/q_{CO2} = 0.011$, confirming the very high selectivity of the adsorbent to remove CO_2 from a natural gas stream.

4.2. Benchmark VSA-PSA Experiments. Once the adsorbent was characterized and the mathematical model for the fixed-bed behavior of the mixture was validated, the following step is the validation of a lab-scale VSA-PSA process for CO_2 removal.

Two main advantages of this process arise from the high selectivity to carbon dioxide and to production of methane at high pressure diminishing pressure drop as much as possible. Both advantages are considered using a four-step Skarstrom-type cycle to separate carbon dioxide from the $CH_4-CO_2-N_2$ ternary mixture. This cycle comprises countercurrent pressurization with methane, feed (where purified methane is obtained as product at high pressure), countercurrent blowdown at low pressure to partially regenerate the adsorbent, and countercurrent purge at low pressure with methane to displace carbon dioxide from the product end. A schematic diagram of the cycle is shown in Figure 6.

Table 5. Experimental Conditions and Parameters Used in VSA-PSA Experiments for the Removal of CO_2 from Natural Gas with a Feed Mixture with CH_4 (60%)/CO_2 (20%)/N_2 (20%) Using Zeolite 13X (CECA)

parameter	$T = 301$ K	$T = 323$ K
feed flowrate, SLPM	4.00	2.07
purge flowrate, SLPM	0.50	0.50
feed pressure, kPa	500/320	500
blowdown pressure, kPa	10	10
axial dispersion coefficient, cm^2/s[a]	2.8	2.7
film mass transfer coefficient, cm/s	$CH_4 = 1.28$ $CO_2 = 1.13$ $N_2 = 1.51$	$CH_4 = 1.16$ $CO_2 = 1.02$ $N_2 = 1.37$
Reynolds number[a]	3.9	2.2
Schmidt number[a]	4.5	4.5
film heat transfer coefficient (gas−solid), $W/m^2 \cdot K$	73	76
film heat transfer coefficient (gas-column wall), $W/m^2 \cdot K$	48	52
global heat transfer coefficient, $W/m^2 \cdot K$	68	71

[a] Values calculated for feed conditions. Equations employed in the calculations are presented elsewhere.[21]

To test the process under different conditions, four different experiments of VSA-PSA were performed. Two different temperatures, ambient (between 298 and 302 K) and 323 K, were used, and also, two different feed step times were tested. The total feed pressure was kept constant at 500 kPa except in one experiment (at 320 kPa), while blowdown pressure was always 10 kPa. Higher flowrates for pressurization and feed steps (4.00 SLPM) were used at ambient temperature compared with 2.07 SLPM used at 323 K. The experimental conditions are presented in Table 5 together with several calculated heat

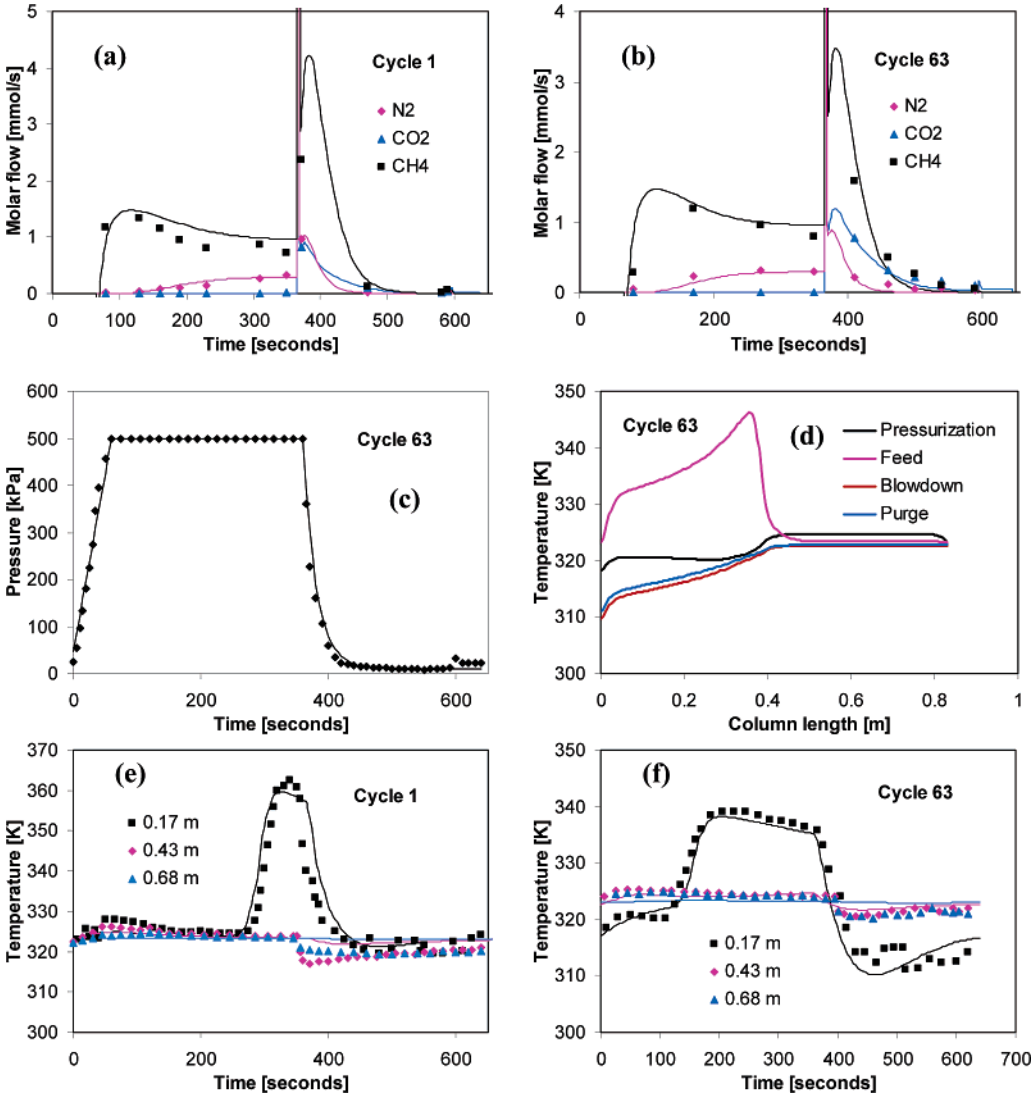

Figure 7. PSA experiment for methane−carbon dioxide−nitrogen separation (run 1, Table 6): molar flowrate of pure gases in cycle 1 (a) and in cycle 63 (b), history of pressure at the exit of the column in the CSS (c), profile of temperature at the end of each step in the CSS (d), and profile of temperature at three different points in the column (0.17, 0.43, and 0.68 m) for cycle 1 (e) and cycle 63 (f).

Table 6. Process Parameters (Step Times, Pressures, and Temperature) of CO_2 Removal by VSA-PSA Using Zeolite 13X from a Mixture of CH_4 (60%)/CO_2 (20%)/N_2 (20%)

run[a]	t_{press}, s	t_{feed}, s	t_{blow}, s	P_{high}, kPa	Q_{press}, SLPM	purity CH_4, %	% CO_2 product	recovery CH_4, %
1[b]	65	300	230	500	2.07	85.73	0.00	27.08
2[b]	65	550	230	500	2.07	78.70	1.76	78.59
3[c]	65	300	230	500	3.50	78.60	1.90	80.33
4[c]	35	300	230	320	3.50	73.10	6.00	88.30

[a] Purge step: 50 s. Purge flowrate: 0.05 SLPM of pure methane. Blowdown pressure: $P_{low} = 10$ kPa. [b] $T = 323$ K. [c] $T = 299$ K.

and mass transfer coefficients used in the mathematical model for the dynamic simulations of the cyclic process.

In Figure 7, the results obtained in the initial run performed at 323 K are shown. Molar flowrates of gases at the exit of the column and temperature histories at three different points in the column are presented for the initial cycle and for cycle 63 when the cyclic steady state (CSS) was reached. The pressure swing at the product end of the column is also plotted as well as the simulated thermal state of the column at the end of each step in CSS. In the first cycle, a temperature increase of 40 K was observed in the first thermocouple at 0.17 m from the feed inlet. This release of a large amount of heat ($-\Delta H = 54.729$ kJ/mol) is due to the high steepness of the adsorption isotherm of CO_2. This peak is much smaller in the following cycles, since the steeper initial part of the isotherms does not belong to the cycle of adsorption−desorption in the cyclic steady state.

Step times as well as performance parameters are detailed in Table 6. The lines in Figure 7 correspond to the predictions of the mathematical model. It can be observed from Figure 7b that no carbon dioxide exits the column in the feed step and thus the product has no CO_2 contamination. The methane recovery in this experiment is very low (27%) due to large losses of methane in the blowdown step. To analyze what can be improved in the process, in Figure 8, we present the simulated amount adsorbed of the three gases at the end of each step in the CSS. It can be observed that, at the end of the feed step, only half of the column was used to adsorb CO_2 while the rest is filled with methane and nitrogen. With this bad utilization of

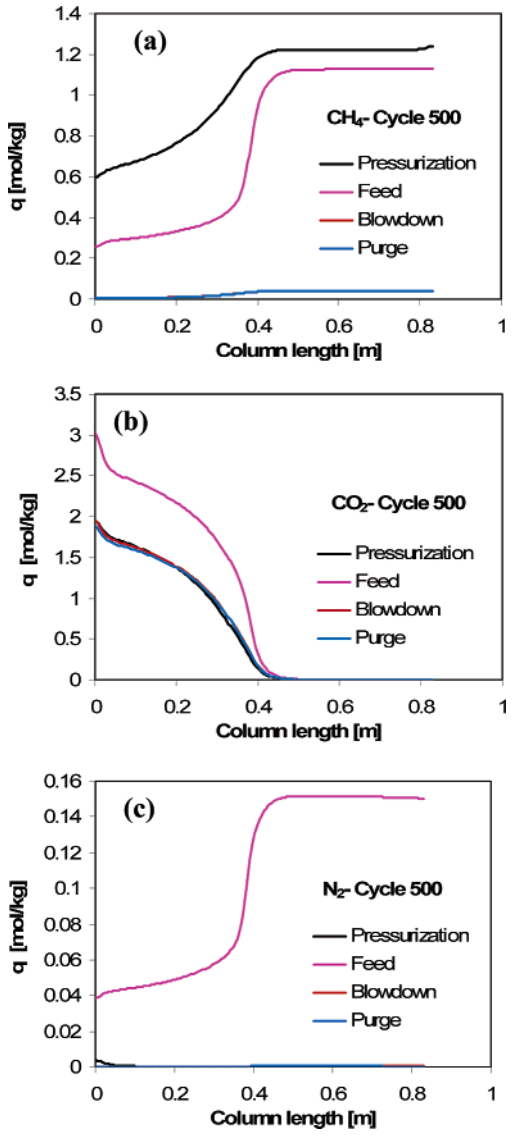

Figure 8. Simulated adsorbed phase concentration profiles at the end of each step for methane (a), carbon dioxide (b), and nitrogen (c) when the CSS was achieved in run 1.

the column for removal of CO_2, the methane inside the column (adsorbed and in the gas phase) at the end of the feed step will be lost in the blowdown, decreasing recovery. A solution to this problem is to increase the amount of feed stream to adsorb more CO_2 in the column. In this work, we kept the flowrate constant and increased the feed step time. We have used a feed step time of 550 s (termed as run 2), almost treating double the amount of gas that was treated in the first experiment.

Another process parameter that was studied in this work was temperature. Other experiments were performed at ambient temperature (299 K). As the amount of CO_2 adsorbed at low temperature is higher, the flowrate of the pressurization and feed steps was increased to 3.50 SLPM. In Figure 9, we present the experimental and predicted (solid lines) results obtained in run 3. It can be observed that almost no CO_2 is exiting the column in the feed step and the amount of methane lost in the blowdown step has drastically decreased, and for this reason, a recovery of methane of 80% was obtained (see Table 6). The low value of purity of CH_4 reported in Table 6 corresponds to methane and nitrogen only with 1.9% CO_2. In the simulation of the temperature profiles at the end of each step in cycle 59 (cyclic steady state), the variation of temperature between the feed and blowdown steps is less than 20 K in the entire column.

Experiments were performed for different feed pressures (500 and 320 kPa). Plots of the molar flowrates in the CSS and the thermal histories in the three thermocouples inside the column for the experiment using a feed with 320 kPa (run 4 in Table 6) are shown in Figure 10. The performance of both experiments (performed with different inlet pressures of 500 and 320 kPa) is reported in Table 6. It can be observed that when using a lower feed pressure there is a large CO_2 contamination of the product with CO_2 (6%). At 500 kPa, the CO_2 content of the product stream is less than 2% under the conditions tested with recovery above 80%.

An increase in the temperature (323 K compared with 300 K) leads to a smaller absolute capacity of carbon dioxide in the zeolite 13X, but the steepness of the isotherm is reduced in such a way that in the pressure range employed in the benchmark experiments, the net amount of carbon dioxide adsorbed per cycle is higher. Also, the amount of heat released per cycle is much smaller, reducing temperature oscillations and thus increasing column capacity.

From these benchmark experiments, it was concluded that the process can be used to remove CO_2 from natural gas streams. The model mixture has a high molar fraction of nitrogen (20%) that also must be diminished to lower values to satisfy the requirements of pipeline grade methane. After this removal process, at least two options are available: the product stream is blended with a purer stream (nitrogen dilution) or goes to the nitrogen rejection unit (NRU) to remove nitrogen prior to injection in the pipeline network.

4.3. VSA-PSA Continuous Operation and Scale-up Considerations. The process proposed in this work has to be arranged in such a way that continuous delivery of product should be obtained. This means that a multicolumn system should be designed. The results shown in Table 6 have some differences with an industrial application of this process. For this reason, to extend the VSA-PSA process to process industrial streams, we have to consider at least three differences with the benchmark experiments:

(a) *Cycle modification*: Most of the losses of methane in the cycle proposed above happen in the blowdown step. To increase methane recovery, it is necessary to include after the feed step a column depressurization to intermediate pressure to avoid serious losses of product, affecting as little as possible the product purity by CO_2 desorption.

(b) *Adiabatic operation*: An industrial VSA-PSA process will work in adiabatic mode. As a result of this, the temperature inside the columns will behave differently than in the laboratory experiments, affecting the process performance.

(c) *Dirty streams for pressurization and purge*: The streams to be used in pressurization and purge steps are not pure methane as used in the benchmark experiments. In multicolumn units, the product streams are used for internal recycles (purge and pressurization) and they can contain different concentrations of contaminants (up to 2% of CO_2) with unwanted consequences for process performance.

To approximate the proposed process to the industrial behavior and compare unit performance parameters with the benchmark experiments, we performed several new process simulations including an intermediate depressurization step and considering adiabatic operation while keeping the molar composition as the following: 60% CH_4, 20% CO_2, and 20% N_2.

The first step was to include an intermediate depressurization step after the feed step. In the depressurization step, the objective is to obtain methane almost free of CO_2 only to increase product recovery. In fact, with a ratio $P_{high}/P_{low} = 50$, large losses of

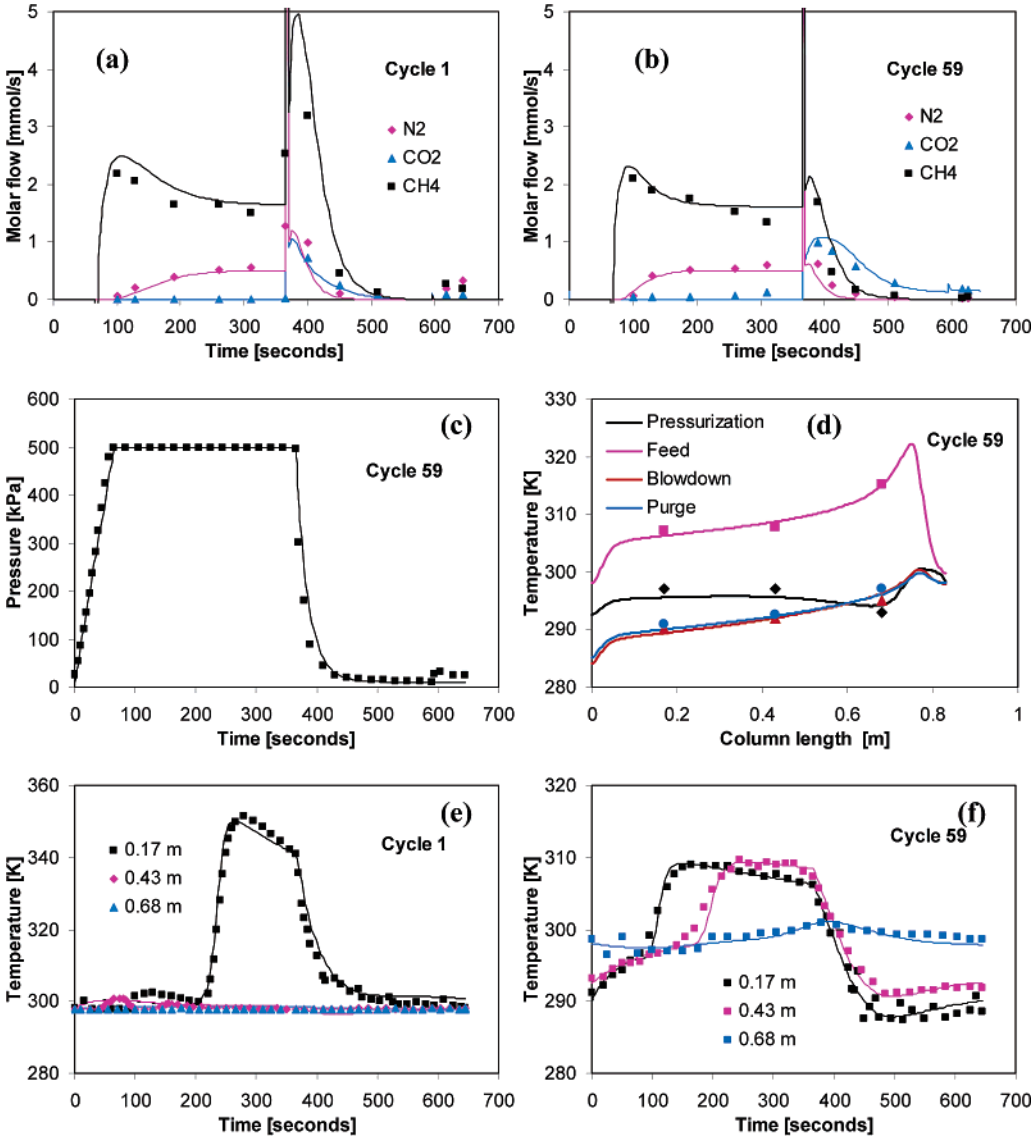

Figure 9. PSA experiment for methane−carbon dioxide−nitrogen separation (run 3, Table 6): molar flowrate of pure gases in cycle 1 (a) and in cycle 59 (b), history of pressure at the exit of the column in the CSS (c), profile of temperature at the end of each step in the CSS (d), and profile of temperature at three different points in the column (0.17, 0.43, and 0.68 m) for cycle 1 (e) and cycle 59 (f).

Table 7. Process Parameters (Step Times, Pressures, and Temperature) of CO_2 Removal by VSA-PSA Using Zeolite 13X from a Mixture of CH_4 (60%)/CO_2 (20%)/N_2 (20%)[a]

run	U, W/m^2·K	purity CH_4, %	% CO_2 product	recovery CH_4, %
S1	80.0	80.29	1.18	88.06
S2	0.0	79.04	2.88	90.16
S3	5000	83.24	0.009	67.41
S4	5000	78.64	0.66	91.42

[a] Operating conditions: $T = 299$ K; feed pressure 500 kPa; feed flowrate 3.5 SLPM; purge step 50 s; purge flowrate 0.1 SLPM of pure methane; blowdown pressure $P_{low} = 10$ kPa. Step times were fixed at 65 s for pressurization, 280 s for feed, 10 s for intermediate depressurization, 230 s for blowdown, and 50 s for purge. In S4, the feed step was 480 s.

methane are expected when reducing the pressure. We have employed a depressurization step to a pressure of 150 kPa as an example, reducing the P_{inter}/P_{low} ratio to 15. In this intermediate depressurization step, the CO_2 concentration profile will move toward the product end ($z = L_c$), and for this reason, less feed can be processed if the same purity of product is to be maintained. We have employed the same operating conditions and process variables as in run 3 (see Table 6) but using a feed step of 280 s (7% less feed per cycle) and including the intermediate depressurization step with a duration of 10 s. The depressurization step has to be fast to avoid CO_2 desorption. The results obtained with this new cycle are summarized in Table 7 (simulation 1, termed as S1). It can be observed that purity of CH_4 is still high with only 1.2% of CO_2 in the product stream but the recovery of methane has increased almost up to 90%.

Another important variable when dealing with CO_2 removal from the gas phase using zeolite 13X is heat transfer. In Figure 1, we showed a temperature peak of almost 80 K using pure CO_2. Also, in all the runs reported in Table 6, temperature oscillations around 20 K per cycle were observed in a nonisothermal, nonadiabatic column. It has to be expected that while operating in an adiabatic regime, some important differences may take place. We have performed two different simulations modifying the global heat transfer coefficient in order to obtain the behavior of the system under adiabatic operation and under near-isothermal operation. The results obtained are compared also in Table 7. It is very important to notice that the thermal regime of operation of the VSA-PSA process is very important in the control of the amount of CO_2 in the product stream: when operating under an adiabatic regime, almost 3% of CO_2 is obtained in the purified stream of methane while less than 0.1%

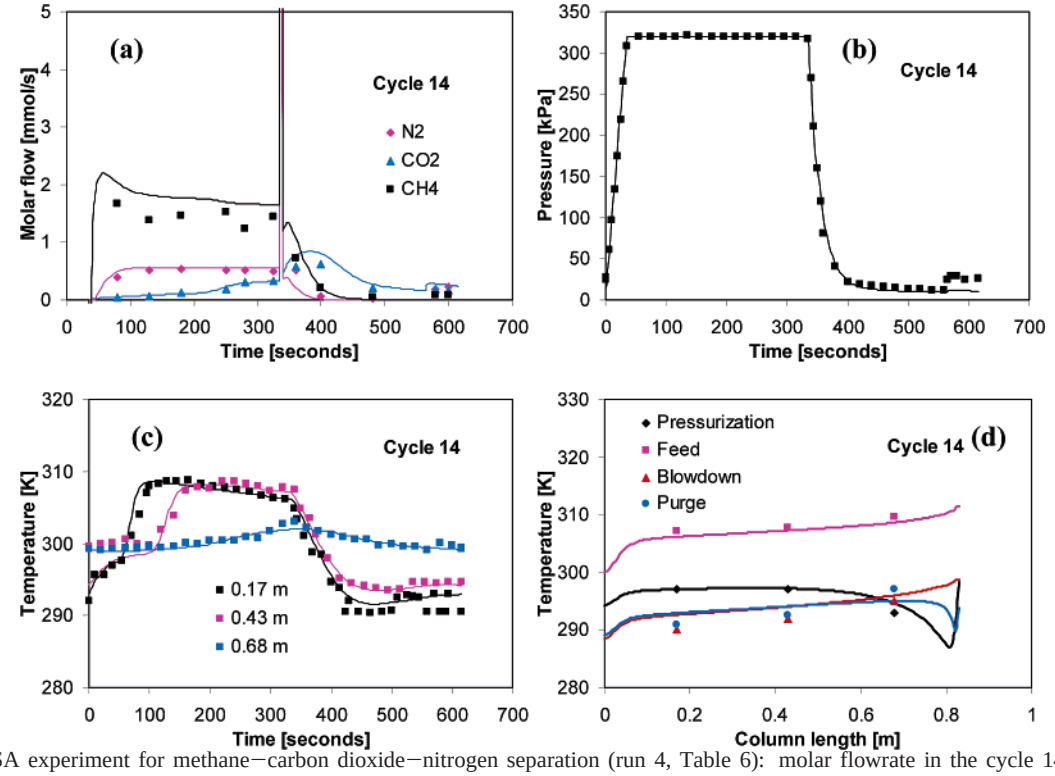

Figure 10. PSA experiment for methane−carbon dioxide−nitrogen separation (run 4, Table 6): molar flowrate in the cycle 14 (a), history of pressure at the exit of the column in cycle 14 (b), profile of temperature at three different points in the column (0.17, 0.43, and 0.68 m) for cycle 14 (c), and profile of temperature at the end of each step for cycle 14 (d).

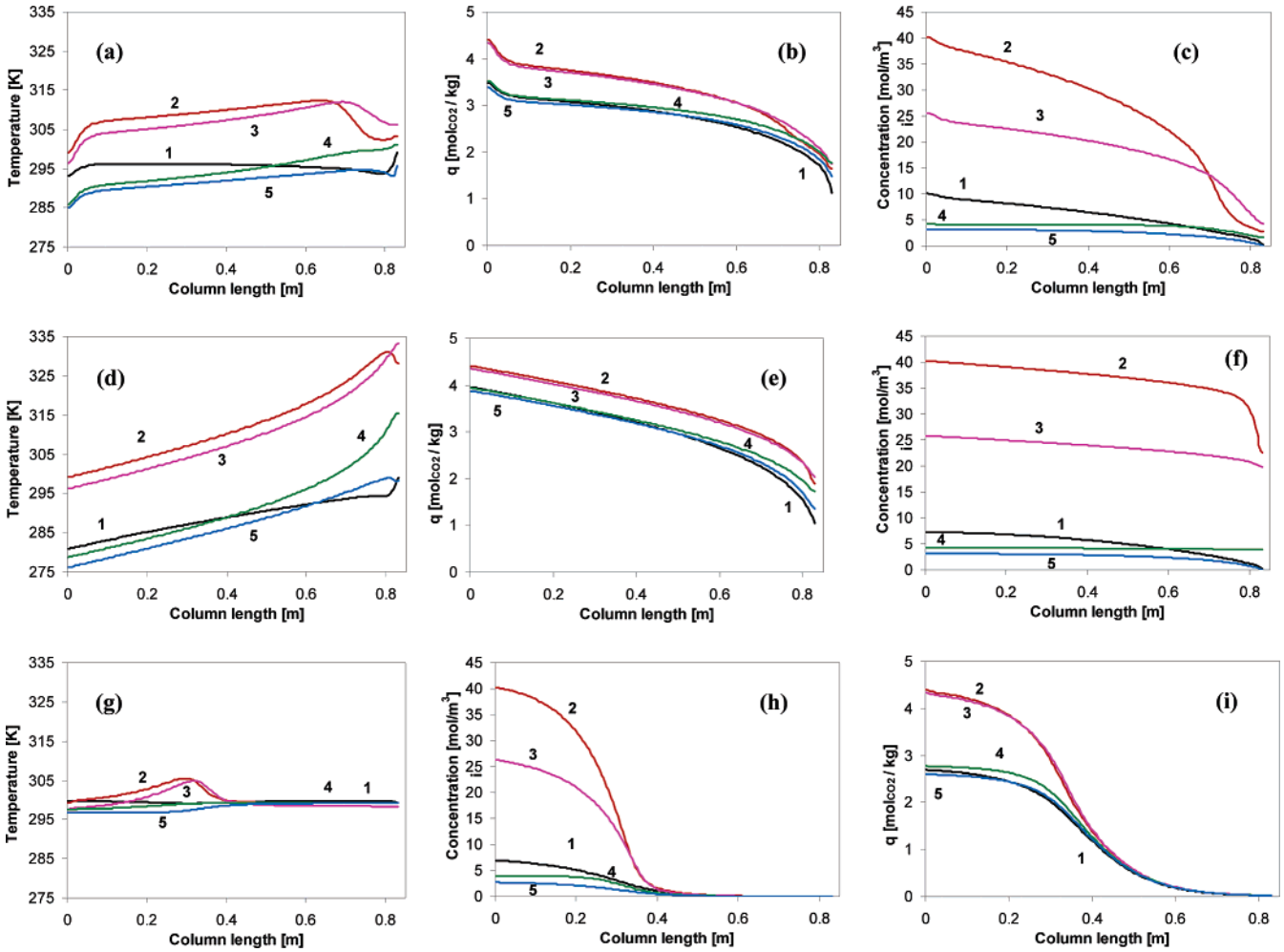

Figure 11. Temperature and adsorbed and gas-phase concentration of CO_2 for VSA-PSA using zeolite 13X to remove carbon dioxide from a mixture 60% CH_4/20% CO_2/20% N_2. The simulation conditions are detailed in Table 7: (a−c) simulation 1, nonadiabatic, nonisothermal; (d−f) simulation 2, adiabatic; (g−i) simulation 3, near-isothermal.

is obtained in the near-isothermal regime. In Figure 11, we show the temperature profiles, gas concentration, and adsorbed phase concentration of CO_2 at the end of each step operating in the cyclic steady state for the near-isotherm simulation, the process using the laboratory determined heat transfer parameters and the adiabatic case. It can be observed in these images that the adsorbed phase concentration of carbon dioxide is almost the same at the end of the feed step and at the end of the intermediate depressurization step, indicating that no CO_2 desorption is occurring in this step as desired.

It has to be mentioned that, in the adiabatic example, the purity of methane can be improved by modifying the step times or inlet flowrates but this will lead to a decrease in unit productivity. On the other side, if heat transfer from the column can be enhanced, unit productivity will also increase. From the concentration profiles showed in Figure 11, it can be observed that the column can process more feed, increasing methane recovery. In Table 7, we show the results of increasing the feed to almost 71% while keeping carbon dioxide under 2% with a recovery around 90%.

With these results, it can be concluded that the possible initial higher costs of heat-exchanged columns for the VSA-PSA process proposed can produce benefits in a long time scale if compared with the classic adiabatic operation of VSA-PSA columns.

5. Conclusions

In this manuscript, we have evaluated a vacuum pressure swing adsorption (VSA-PSA) process for the removal of carbon dioxide in a contaminated stream of natural gas to achieve fuel grade methane. The adsorbent used was zeolite 13X (CECA) where CO_2 is selectively adsorbed. A Skarstrom-type cycle comprising countercurrent pressurization with product, feed, countercurrent blowdown, and countercurrent purge was tested in benchmark experiments with a mixture having 60% CH_4/20% CO_2/20% N_2. Process variables such as temperatures and flowrates were evaluated in a single-column VSA-PSA unit. Under the conditions tested, CO_2 was removed to levels lower than 2% as required by fuel grade methane with methane recovery of 80.3%. Process simulations of a five-step cycle (countercurrent pressurization with product, feed, intermediate depressurization, countercurrent blowdown, and countercurrent purge) were also performed, improving methane recovery to values around 90%. Simulations modifying the heat transfer parameters of the column were also performed. It was noted that the thermal regime of operation of the VSA-PSA process is very important in the control of the amount of CO_2 in the product stream. It was determined that initially higher costs for heat-exchanged columns for the VSA-PSA process, which operate at nearly isothermal conditions, may produce benefits in the long run as compared to the classic adiabatic operation of VSA-PSA columns.

Acknowledgment. The authors would like to thank the Foundation for Science and Technology (FCT) for financial support via project POCTI/EQU/59330/2004 and CECA for providing the adsorbent. S.C. acknowledges FCT grant SFRH/BPD/21019/2004.

Nomenclature

a' = area-to-volume ratio (1/m)
a_i = number of neighboring sites occupied by a molecule of component i
$Bi_{,i}$ = Biot number of componente i
$\bar{c}_i$ = averaged concentration in the macropores for component i (mol/m^3)
C = concentration (mol/m^3)
C_i = concentration of component i in the gas phase (mol/m^3)
$\tilde{C}_p$ = molar constant pressure specific heat of the gas mixture (J/mol·K)
$\tilde{C}_{ps}$ = constant pressure specific heat of the adsorbent (J/kg·K)
$\tilde{C}_{pw}$ = specific heat of the column wall (J/kg·K)
$\tilde{C}_v$ = molar constant volumetric specific heat of the gas mixture (J/mol·K)
$\tilde{C}_{vi}$ = molar constant volumetric specific heat of component i (J/mol·K)
$\tilde{C}_{v,ads,i_i}$ = molar constant volumetric specific heat of component i adsorbed (J/mol·K)
C_t = total gas concentration (mol/m^3)
d_p = pellet diameter (m)
D_{ax} = axial dispersion coefficient (m^2/s)
$D_{p,i}$ = pore diffusivity of component i (m^2/s)
$D_{m,i}$ = molecular diffusivity of component i (m^2/s)
$D_{k,i}$ = Knudsen diffusivity of component i (cm^2/s)
D_w = internal diameter of the column (m)
$D_{\mu,i}$ = crystal diffusivity of component i (m^2/s)
$\mathcal{D}_{\mu,i}$ = limiting diffusivity at infinite temperatures for component i (m^2/s)
e = wall thickness (m)
$E_{a,i}$ = activation energy of micropore diffusion for component i (kJ/mol)
h_f = film heat transfer coefficient between the gas and the solid phase (W/m^2·K)
h_w = film heat transfer coefficient between the gas phase and the column wall (W/m^2·K)
k_{fi} = film mass transfer coefficient (m/s)
K_i = adsorption equilibrium constant of component i (1/kPa)
K_i° = adsorption equilibrium constant at the limit $T \rightarrow \infty$ of component i (1/kPa)
$K_{\mu,i}$ = LDF constant for mass transfer in the micropores for component i (m/s)
$K_{p,i}$ = LDF constant for mass transfer in the macropores for component i (m/s)
L_c = column length (m)
N = total mass flux from gas phase to solid boundary (mol/m^3·s)
P = total pressure (1/kPa)
P_{blow} = total pressure (1/kPa)
P_{feed} = feed pressure (1/kPa)
P_{high} = high pressure (1/kPa)
P_{inter} = intermediate pressure (1/kPa)
P_{low} = low pressure (1/kPa)
q_i = adsorbed phase concentration of component i (mol/kg)
q_i* = adsorbed gas-phase concentration in the equilibrium state of component i (mol/kg)
$\langle \bar{q}_i \rangle$ = extrudate averaged adsorbed phase concentration (mol/kg)
$q_{max,i}$ = saturation capacity of component i (mol/kg)
Q_{feed} = feed flowrate, SLPM (l/min)
Q_{press} = pressurization flowrate, SLPM (l/min)
Q_{purge} = purge flowrate, SLPM (l/min)
r_c = radius of the crystal (m)
R_c = radius of the column (m)
R_{ey} = Reynolds number
R_p = radius of the extrudate (m)
R_g = universal gas constant (J/mol·K)
R_w = radius of the wall (m)
S_{ch} = Schimdt number
t = time (s)
t_{cycle} = total cycle time (s)
t_{feed} = feed step time (s)
t_{intdep} = intermediate depressurization step time (s)
t_{blow} = countercurrent blowdown step time (s)
t_{press} = pressurization step time (s)
t_{purge} = purge step time (s)
t_{total} = total time (s)
T = temperature (K)

T_g = temperature of the gas phase (K)
T_s = temperature of the solid phase (K)
T_w = wall temperature (K)
T_∞ = temperature to fix the oven (K)
u = superficial velocity of component i (m/s)
U = global external heat transfer coefficient (W/m^2·K)
y_i = molar fraction of component i
z = axial distance along the column (m)

Greek Letters

α_w = ratio of the internal surface area to the volume of the column wall (1/m)
α_{wl} = ratio of the logarithmic mean surface area of the column shell to the volume of the column wall (1/m)
ρ_b = gas density in the bulk (kg/m^3)
ρ_c = column density (kg/m^3)
ρ_g = gas density (kg/m^3)
ρ_p = extrudate density (kg/m^3)
ρ_w = column wall density (kg/m^3)
λ = axial heat dispersion (W/m^2·K)
$(-\Delta H_i)$ = isosteric heat of adsorption of component i (kJ/mol)
ϵ = porosity
ϵ_c = porosity of the column
ϵ_p = porosity of the extrudate
τ_e = extrudate tortuosity
τ_p = pore tortuosity
ω_c = crystal weight fraction of the extrudate
μ_g = gas viscosity (Pa.s)

EF060119E